

MIT Open Access Articles

*The effect of excess atomic volume on He
bubble formation at fcc-bcc interfaces*

The MIT Faculty has made this article openly available. **Please share**
how this access benefits you. Your story matters.

Citation: Demkowicz, M. J. et al. "The effect of excess atomic volume on He bubble formation at fcc-bcc interfaces." Applied Physics Letters 97.16 (2010): 161903.

As Published: <http://dx.doi.org/10.1063/1.3502594>

Publisher: American Institute of Physics

Persistent URL: <http://hdl.handle.net/1721.1/69035>

Version: Author's final manuscript: final author's manuscript post peer review, without publisher's formatting or copy editing

Terms of use: Creative Commons Attribution-Noncommercial-Share Alike 3.0



The effect of excess atomic volume on He bubble formation at fcc-bcc interfaces

M. J. Demkowicz^{1,*}, D. Bhattacharyya², I. Usov³, Y. Q. Wang³, M. Nastasi², A. Misra²

¹Materials Science and Engineering Department, Massachusetts Institute of Technology, Cambridge, MA 02139

²Center for Integrated Nanotechnologies, Los Alamos National Laboratory, Los Alamos, NM 87545

³MST-8: Structure-Property Relations Group, Los Alamos National Laboratory, Los Alamos, NM 87545

Abstract

Atomistic modeling shows that Cu-Nb and Cu-V interfaces contain high excess atomic volume due to constitutional vacancy concentrations of $\sim 5\%$ at. and $\sim 0.8\%$ at., respectively. This finding is supported by experiments demonstrating that a ~ 5 -fold higher He concentration is required to observe He bubbles via through-focus transmission electron microscopy at Cu-Nb interfaces than in Cu-V interfaces. Interfaces with structures tailored to minimize precipitation and growth of He bubbles may be used to design damage-resistant composites for fusion reactors.

Unlike pure metals¹, some materials contain constitutional vacancies that are thermodynamically stable at arbitrarily low temperature, for example grain boundaries (GBs) in ceramics² and semiconductors³, compounds with wide phase fields like NiAl⁴, and certain metal hydrides⁵. We use atomistic modeling to show that Cu-Nb and Cu-V interfaces contain high constitutional vacancy concentrations. Indirect experimental verification of this prediction is obtained by measuring the critical He concentration at which bubbles become detectable at these interfaces in transmission electron microscopy (TEM).

* Corresponding author: demkowicz@mit.edu

All the heterointerfaces in magnetron sputtered Cu-Nb and Cu-V multilayers form along close packed fcc and bcc planes and purely in the Kurdjumov-Sachs (KS) orientation relation⁶: a $\langle 110 \rangle$ direction in the (111) fcc interface plane is parallel to a $\langle 111 \rangle$ direction in the (110) bcc interface plane, as in Fig. 1.a). Figure 1.b) shows a plan view of the Cu-Nb interface in a model that was relaxed using a specially constructed embedded atom method (EAM) potential⁷. While not strictly periodic, this interface contains a quasi-periodic pattern of sites where a Cu and Nb atom are nearly “on top” of each other. These sites occur at the intersections between two sets of parallel interface misfit dislocations, as elaborated elsewhere^{8,9}.

Figure 1.c) demonstrates the effect of removing an atom (creating a vacancy) near a misfit dislocation intersection in the interface Cu plane. The formation energy of the unrelaxed vacancy is 1.5eV, comparable to fcc Cu (1.3eV¹). Upon annealing for 10ps at 300K followed by energy minimization, the vacancy reconstructs into the configuration in Fig. 1.d) and its formation energy drops to -0.13eV. Thus, the structure in Fig. 1.d) is energetically favorable to the vacancy-free interface in Fig. 1.b) and the reconstructed vacancy may be viewed as a constitutional vacancy.

To find the ground state interface, we iteratively add vacancies until no negative formation energy sites remain. For Cu-Nb, this structure is shown in Fig. 1.e). It has $\sim 25\text{mJ/m}^2$ lower energy than that in Fig. 1.b) and contains 5%at. constitutional vacancies concentrated near misfit dislocation intersections, i.e. ~ 2.5 vacancies per intersection. A similar calculation for a Cu-V interface also shows ~ 2.5 vacancies per intersection and an energy reduction of $\sim 3.4\text{mJ/m}^2$. Due to the differing lattice parameters of Nb and V, however, the areal density of misfit dislocation intersections in Cu-V is smaller, giving an overall $\sim 0.8\%$ at. constitutional vacancy concentration, shown in Fig. 1.f).

These theoretical predictions may be indirectly verified by quantifying the He solubility limits at Cu-Nb and Cu-V interfaces. In perfect crystalline metals, formation energies of He interstitials are close to self-interstitial formation

energies^{10,11}. Consequently, He solubility is below one part per trillion even near the melting temperature¹². He therefore preferentially occupies high excess volume sites like vacancies and vacancy clusters. Due to their constitutional vacancies, both Cu-Nb and Cu-V interfaces have high excess volume (verified by Voronoi tessellation¹³) and thus may exhibit elevated He solubility compared to perfect crystalline metals. Furthermore, the solubility limit should be higher in Cu-Nb than in Cu-V interfaces.

Experimental measurement of He solubility at interfaces poses serious challenges: both local He concentration and whether He has precipitated out must be determined. Due to high solubility, the He concentration needed to nucleate bubbles may be increased compared to the bulk, meaning that He could be present in supersaturation without precipitating. Furthermore, TEM might not be able to resolve the smallest, incipient clusters formed in the early stages of precipitation. Thus, rather than attempt a precision measurement of He solubility itself, we measured the critical He concentration at which bubbles are unambiguously detected via through-focus imaging in TEM: a quantity that, like solubility, should scale with interface excess volume.

Two Cu-Nb multilayers were magnetron sputtered onto Si substrates, as in previous studies¹⁴: one with 335nm overall thickness and 5.6nm-thick layers and another 340nm-thick with 2.8nm layers. These samples were implanted at room temperature with 35keV He³ with $10^{17}/\text{cm}^2$. To reduce channeling, samples were tilted 7 degrees from the incident ion beam. He³ concentration as a function of depth was measured using nuclear reaction analysis (NRA), in which atoms in an incident deuterium beam react with implanted He³ to produce alpha particles and protons. NRA provides substantially higher depth resolution than methods like elastic recoil detection (ERD) or secondary ion mass spectrometry (SIMS)¹⁵. He³ depth profiles were computed from alpha particle energies using SIMNRA¹⁶. The stopping power of implanted He³ was neglected in the analysis. The concentration uncertainty near

the surface, $\sim 0.2/\text{nm}^3$, was used as a concentration uncertainty estimate throughout the sample depth. The detection limit was $\sim 0.5/\text{nm}^3$.

He bubbles in 100nm foils taken from the implanted samples were examined using through-focus bright field (BF) imaging in TEM. Figure 2 shows an under focused BFTEM image where bubbles appear as white dots (dark in over focus, not shown). The diameters of the smallest detectable bubbles were estimated at $\sim 1\text{nm}$ from images at different defocus using the approach outlined in¹⁷. In the 5.6nm layer sample numerous bubbles formed at depths containing high He³ concentration with the number decreasing in the low concentration tails. Visual inspection shows no bubbles below a critical depth of $215\pm 10\text{nm}$, even though the measured He³ concentration there is $1.4\pm 0.6/\text{nm}^3$ ($\sim 1.7\text{at.}\%$), as inferred by comparing the TEM image with the measured concentration profile in Figure 2. At greater depths the He³ concentration is too low to form the $\sim 1\text{nm}$ bubbles resolvable elsewhere in the sample. The critical concentration $1.4\pm 0.6/\text{nm}^3$ is significantly higher than the (immeasurably small) concentration required to observe bubbles in pure fcc and bcc metals, implying that all the implanted He above the critical depth is trapped at interfaces.

Figure 2 also shows that He bubbles did not form within $\sim 25\text{nm}$ of the free surface, even though the He³ concentration there exceeded $1.4\pm 0.6/\text{nm}^3$. This higher critical concentration may be due to trapping of implanted He at radiation-induced vacancies. Such He-vacancy complexes are much less mobile than interstitial He¹¹ and may prevent He from reaching nearby interfaces, especially in multilayers with thick individual layers. The concentration of radiation-induced vacancies decreases with depth faster than that of He, suggesting the critical concentration measured at the end of the implantation range, albeit possibly still an overestimate, better indicates the amount of He trapped at interfaces than the concentration near the free surface.

Further modeling and implantation studies with controlled He/dpa ratios as well as improved TEM techniques to reliably detect He clusters will help resolve the above issue, but additional support for our interpretation may be obtained from the 2.8nm layer sample, whose interface area per unit volume is twice that of the 5.6nm layer sample. If all implanted He above the critical depth is trapped at interfaces, the critical He concentration needed to image bubbles in the 2.8nm layer sample should be twice that of the 5.6nm layer sample, i.e. $2.8 \pm 1.2 / \text{nm}^3$. Indeed, measurements like that in Figure 2 show no He bubbles in the 2.8nm multilayer above a critical depth of $195 \pm 10 \text{nm}$, corresponding to a He concentration of $3.3 \pm 0.6 / \text{nm}^3$, within the uncertainty range of the predicted value.

For samples of layer thicknesses t , the He concentration per unit interface area c_i can be calculated as $c_i = t c_c$, where c_c is the critical He concentration per unit volume, measured above. Averaging the results from the 5.6nm and 2.8nm multilayers, a critical Cu-Nb interface He concentration to resolve bubbles of $8.5 \pm 2.5 / \text{nm}^2$ is obtained. Similar experiments conducted on magnetron sputtered Cu-V multilayers gave a critical He concentration of $\sim 1.9 / \text{nm}^2$ for Cu-V interfaces¹⁸: a factor of ~ 4.5 smaller than in Cu-Nb interfaces, in good agreement with the prediction based on constitutional vacancy concentrations obtained from atomistic modeling.

Materials that contain interfaces with high excess atomic volume may find applications in new structural materials for nuclear fusion. As much as 1500 appm He may be implanted at 10 appm/dpa in the plasma facing walls of tokomaks¹⁹. The subsequent nucleation of He bubbles at GBs promotes void growth and leads to embrittlement²⁰. At large He concentrations and elevated temperatures, bubbles can grow into voids and blisters²¹.

One way to address this problem may be to trap He at nanoscale inclusions, e.g. YTiO clusters in ODS steels²². Another may be to synthesize materials containing interfaces with increased resistance to He-assisted degradation. He bubble formation and He-assisted void growth may be delayed at interfaces with high He

solubility, allowing such materials to remain in service longer than existing structural alloys. Furthermore, if these interfaces can promote He outgassing—as demonstrated in Cu-Nb²³—then He-assisted degradation may be further delayed. The distribution of free volume at fcc-bcc heterophase interfaces likely depends on the orientation relation and the habit plane orientation. Thus, it may be possible to tailor interface-He interactions by adjusting the distribution of interface constitutional vacancies via judicious selection of interface crystallography to control the configuration of misfit dislocation intersections⁹.

We thank R. R. Greco for carrying out He³ implantations, P. Dickerson for TEM sample preparation, and R. G. Hoagland and G. R. Odette for insightful discussions. This research was funded by the Center for Materials in Irradiation and Mechanical Extremes, an Energy Frontier Research Center funded by the U. S. Department of Energy, Office of Science, Office of Basic Energy Sciences under award number 2008LANL1026. Support from the LANL LDRD program (NRA measurements) is also acknowledged.

Figures

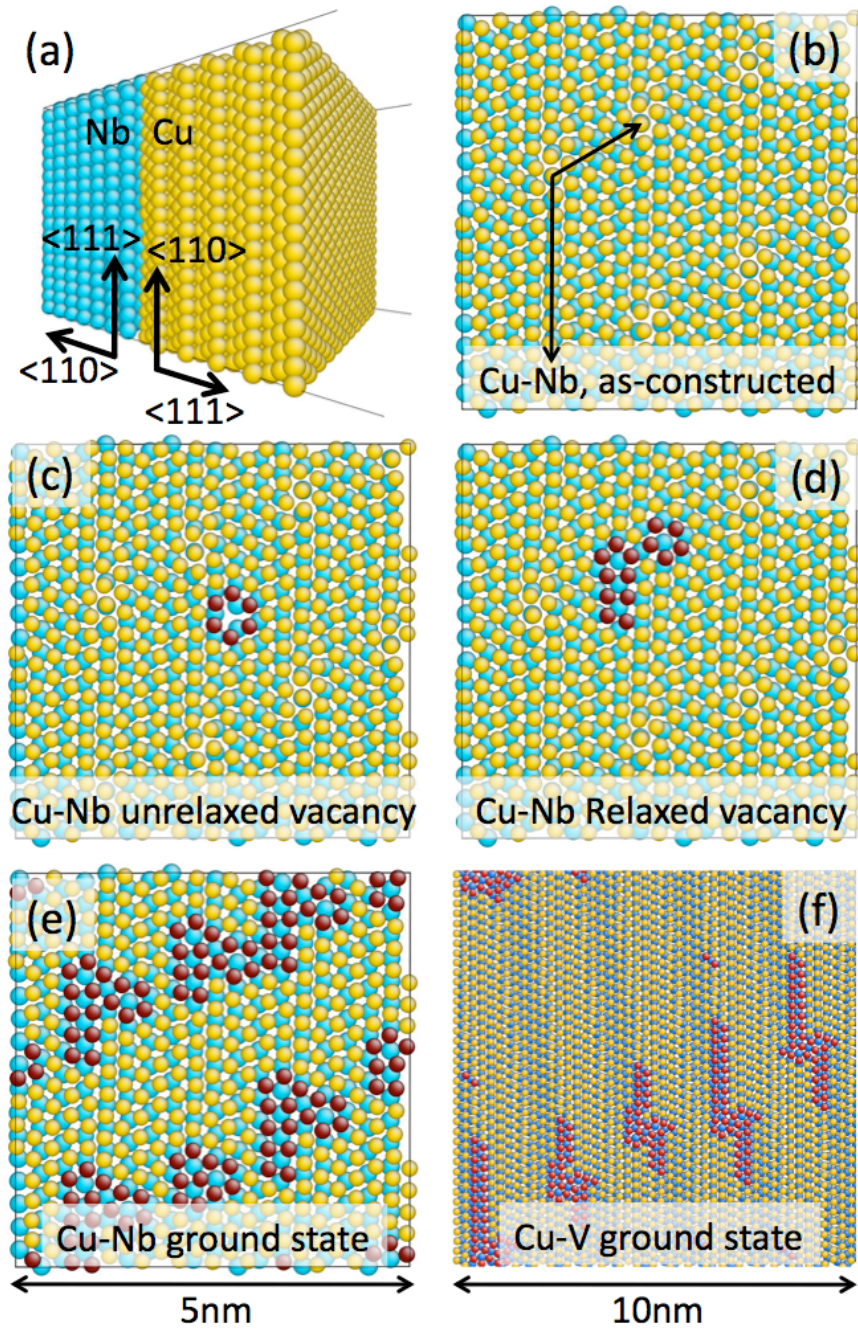


Figure 1: (a) Cu-Nb bilayer in the experimentally-observed crystallography⁶, (b) quasi-periodic pattern formed by interface Cu and Nb planes, (c) unrelaxed interface vacancy, (d) relaxed interface vacancy, (e) ground state Cu-Nb interface with 5%at. constitutional vacancies, (f) ground state Cu-V interface with ~0.8%at. constitutional vacancies. Atoms colored red have less than 6 nearest neighbors in the interface Cu plane.

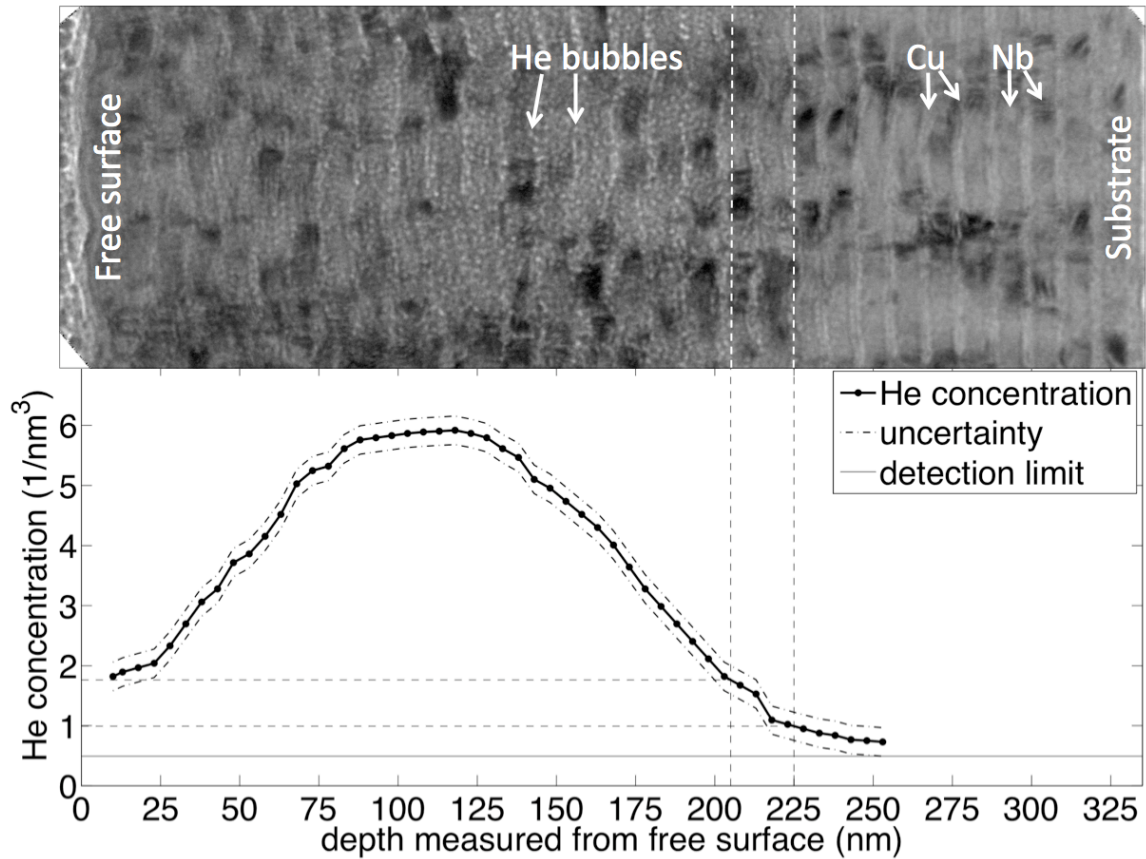


Figure 2: BFTEM image at $\sim 1\mu\text{m}$ under focus of He^3 -implanted Cu-Nb multilayers with 5.6nm-thick layers (top) and the corresponding He concentration profile measured by NRA (bottom). No bubbles are seen below a critical depth of $215\pm 10\text{nm}$ (indicated by dashed lines), corresponding to a He concentration of $1.4\pm 0.6/\text{nm}^3$.

References

- 1 Paul G. Shewmon, *Diffusion in Solids*, 2nd ed. (Minerals, Metals & Materials Society, Warrendale, Pa., 1989).
- 2 Z. L. Zhang, W. Sigle, F. Phillipp et al., *Science* **302**, 846 (2003).
- 3 S. von Althaus, K. Kaski, and A. P. Sutton, *Phys. Rev. B* **74**, 134101 (2006).
- 4 A. J. Bradley and A. Taylor, *Proc. Roy. Soc. Lond.* **159A**, 56 (1937); M. Nastasi, L. S. Hung, H. H. Johnson et al., *J. Appl. Phys.* **57**, 1050 (1985).
- 5 Y. Fukai, *J. Alloy. Compd.* **356-357**, 263 (2002).
- 6 T. E. Mitchell, Y. C. Lu, A. J. Griffin et al., *J. Am. Ceram. Soc.* **80**, 1673 (1997).

- 7 M. J. Demkowicz and R. G. Hoagland, *Int. J. Appl. Mech.* **1**, 421 (2009).
- 8 M. J. Demkowicz, R. G. Hoagland, and J. P. Hirth, *Phys. Rev. Lett.* **100**, 136102
(2008).
- 9 M. J. Demkowicz, J. Wang, and R. G. Hoagland, in *Dislocations in Solids*, edited
by J. P. Hirth (Elsevier, Amsterdam, 2008), Vol. 14, p. 141.
- 10 T. Seletskiaia, Y. Osetsky, R. E. Stoller et al., *Phys. Rev. Lett.* **94**, 046403
(2005).
- 11 C. C. Fu and F. Willaime, *Phys. Rev. B* **72**, 64117 (2005).
- 12 J. Laakmann, P. Jung, and W. Uelhoff, *Acta Metall.* **35**, 2063 (1987).
- 13 Masaharu Tanemura, Tohru Ogawa, and Naofumi Ogita, *J. Comput. Phys.* **51**,
191 (1983).
- 14 P. M. Anderson, J. F. Bingert, A. Misra et al., *Acta Mater.* **51**, 6059 (2003); A.
Misra, R. G. Hoagland, and H. Kung, *Philos. Mag.* **84**, 1021 (2004); T.
Hochbauer, A. Misra, K. Hattar et al., *J. Appl. Phys.* **98**, 123516 (2005).
- 15 F. Paszti, *Nucl. Inst. Meth. B* **66**, 83 (1992).
- 16 M. Mayer, *SIMNRA User's Guide* (Max-Planck-Institut für Plasmaphysik,
Garching, Germany, 1997).
- 17 M. Ruhle and M. Wilkens, *Crystal Lattice Defects* **6**, 129 (1975).
- 18 E. G. Fu and X. Zhang, unpublished (2010).
- 19 S. J. Zinkle, *Phys. Plasmas* **12**, 8 (2005).
- 20 H. Trinkaus and H. Ullmaier, *J. Nucl. Mater.* **212-215**, 303 (1994).
- 21 R. E. Galindo, A. van Veen, J. H. Evans et al., *Nucl. Inst. Meth. B* **217**, 262
(2004).
- 22 T. Yamamoto, G. R. Odette, P. Miao et al., *J. Nucl. Mater.* **367-370**, 399 (2007).
- 23 M. J. Demkowicz, Y. Q. Wang, R. G. Hoagland et al., *Nucl. Inst. Meth. B* **261**, 524
(2007).